Segmentation of Liver Metastases Using a Level Set Method with Spiral-Scanning Technique and Supervised Fuzzy Pixel Classification

Dirk Smeets, Bert Stijnen, Dirk Loeckx, Bart De Dobbelaer, and Paul Suetens

Katholieke Universiteit Leuven
ESAT - PSI
dirk.smeets@gmail.com

Abstract. In this paper a specific method is presented to facilitate the semi-automatic segmentation of liver metastases in CT images. Accurate and reliable segmentation of tumors is e.g. essential for the follow-up of cancer treatment. The core of the algorithm is a level set function. The initialization is provided by a spiral-scanning technique based on dynamic programming. The level set evolves according to a speed image that is the result of a statistical pixel classification algorithm with supervised learning. This method is tested on CT images of the abdomen and compared with manual delineations of liver tumors.

1 Introduction

Segmentation is an image processing operation to distinguish an anatomical structure from the surrounding tissue. Tumor segmentation is an important issue for cancer follow-up, where the oncologist is interested to evaluate the change in size of the tumors. Early response prediction allows the oncologist to adapt the therapy, which can lead to a higher survival rate [1]. Measuring the response of a treatment can be done by uni-, bi- or tridimensional criteria. Clinical research [1–3] indicates that volume measurements (3D) give the best reflection of the tumor response. Volume measurements require the segmentation of the tumors, which is very time consuming when it is done manually. Moreover, manual delineations are subjected to intra- and interobservervariability, which is estimated at about 8% for liver tumors [4]. Therefore, automatic or semi-automatic tumor delineation algorithms are required.

This article focuses on the segmentation of liver tumors in contrast-enhanced CT images. Because tumors generally have different shapes and intensities, the segmentation is not straightforward. The gray values of a tumor depend on the delay between the contrast injection and the image acquisition, the contrast dose and the patient physiology. In general, liver tumors have a more or less round shape. However, the shape can be influenced by the vicinity of blood vessels, the edges of anatomical structures, the type of cancer,...

Several semi-automatic methods are already available for the segmentation of CT liver tumor segmentation. These include methods based on watershed like

the paintbrush algorithm [5, 6], deformable models like the active contour algorithm in [7] and a region growing technique using several constraints [8]. These methods have in common that they all require an extensive amount of user interaction.
The segmentation algorithm described in this paper combines several techniques including a spiral scanning technique, pixel classification and level sets. The spiral scanning technique is based on [9], where it is implemented for lung nodules. Here the implementation is performed on liver tumor segmentation using a different parametrization and a additional gradient to enhance the tumor edges. The pixel classification and level set method are based on the standard implementation for both algorithms.
The algorithm is validated on a test data set provided by "3D Segmentation in the Clinic: A Grand Challenge II" [10] using 5 evaluation measures: volumetric overlap, relative absolute volume difference, average symmetric absolute surface distance, symmetric RMS surface distance and maximum symmetric absolute surface distance.
After this introduction, we first give a detailed description of the method. Next, the validation results are given, followed by a discussion and conclusion.

2 Method

To start, the algorithm requires the user to place one point approximately in the middle of the tumor and specify a maximal radius, which is about two times the largest radius of the tumor. Next, this input is used to generate an initialization for the level set using a spiral-scanning technique [9]. The speed image guiding the propagation of the level set is calculated independently using fuzzy classification. The heart of the algorithm is the standard level set function [11]. After level set segmentation, post-processing is used to transform the distance map into a binary image. An overview of the method is given in Figure 1.

2.1 Initial Segmentation

The initial segmentation is provided by a Spiral-Scanning Technique [9]. This technique transforms the 3D image to 2D space using a scanning technique, allowing us to find a contour using dynamic programming for the segmentation. The 3D image is sampled along scan lines. The endpoints form a spiral on the surface of a sphere starting at the north pole and ending at the south pole. Our parametrization of this spiral is given by

$$x = x_C + \rho \sin(t) \cos(2Nt) \tag{1}$$

$$y = y_C + \rho \sin(t) \sin(2Nt) \tag{2}$$

$$z = z_C + \rho \cos(t) \tag{3}$$

with $t = \frac{\pi}{2} + \arcsin(\frac{2k_1}{2N^2} - 1)$ en $\rho = \frac{\rho_{max} k_2}{M}$. N is the number of rotations, $2N^2$ the number of scan lines and M is the number of samples on each scan

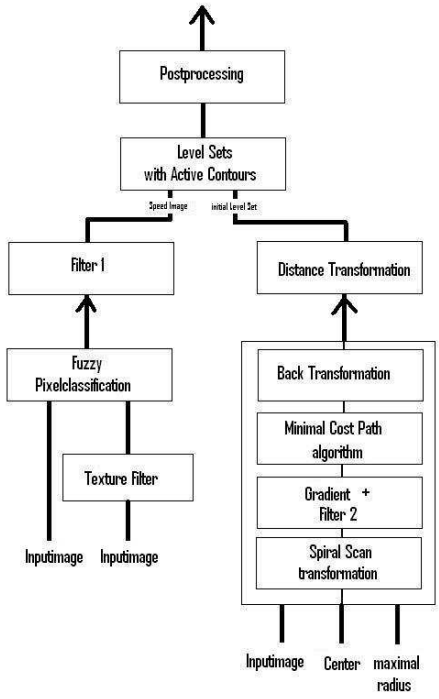

Fig. 1: Block Diagram of Segmentation Algorithm

line, k_1 and k_2 are the coordinates of the 2D space. The result of the spiral-scan transformation is given in Fig. 2.

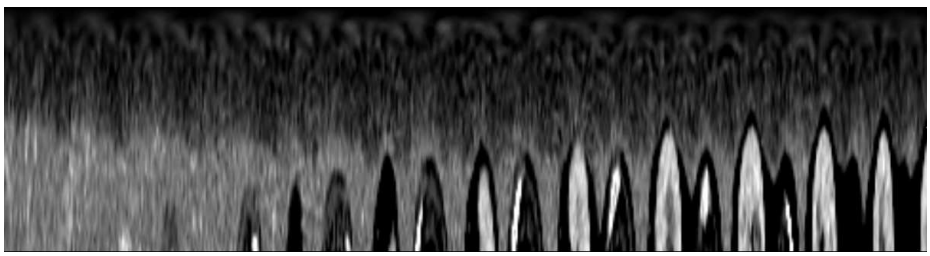

Fig. 2: Scan converted image

In the transformed image, a dynamic programming algorithm performs the actual segmentation. This is done by calculation of the minimal cost path. The sum of internal cost, $E_C^{int}(i) = wt.|y_i - y_{i-1}|$, and the external cost, $E_C^{ex}(i) =$

$|\nabla I|_{max} - |\nabla I(x_i, y_i)|$, is minimized to achieve a curve which separates the image in a tumor and a non-tumor part. Instead of just using the image gradient for the calculation of the external cost, the gradient of a binary image is added to the image gradient in order to enhance the tumor edges. The binary image is simply calculated by applying an interval thresholding operation. The used upper-threshold is chosen as the average of the estimates of the mean gray value of the tumor and the liver in the image. Those estimates are based on the intensity distribution in a sphere with a radius of 10 voxels around the user click respectively in the center of the tumor and outside the tumor.

The result of the dynamic programming algorithm is a 2D binary segmentation. The back transformation to 3D uses the nearest neighbor principle. For each voxel lying on a distance $\rho < \rho_{max}$ from the center of the spiral, the algorithm searches the nearest sample on a spiral with radius ρ.
The final step to achieve an initial level set is a distance transformation. For each voxel, the shortest distance to the surface is calculated and stored. Voxels lying within the segmented surface get a negative value. The result is a signed distance function [12].

2.2 Speed Function

The left branch in Fig. 1 results in a speed image that will deform the initial segmentation to the final result. This speed image is based on supervised fuzzy pixel classification. Fuzzy pixel classification calculates the probability that a certain pixel belongs to a certain image class c_j [13]. Within the liver two classes can be distinguished: liver tissue and tumor tissue. The statistical model uses a normal distribution where the parameters μ and σ are estimated based on the gray values in spheres around the point inside and outside the tumor. To increase reliability, not only the image intensities could be taken into account, but also some texture features [14]. Initial experiments show that correlation and variance could best distinguish liver tissue from tumor tissue, but the computational complexity to calculate the features is too high to allow the use in semi-automatic algorithms. After having calculated the fuzzy image, Filter 1 (see Fig. 1) transforms the image in a speed image by applying

$$I_V(x) = f_3(p(c_{tumor}|I_k)) = |2\ p(c_{tumor}|I_k) - 1|$$

The speed function has high values far from the tumor edges. To reduce noise without eliminating the edges an anisotropic diffusion filter is used to filter the speed image.

2.3 Level Sets

The initial level set is represented by an implicit function $\phi(x, t)$ and deformed under influence of a speed image. For computational reasons, a local level set

method is used, because it defines $\phi(x, t + \delta t)$ only near the zero level set [15]. The partial differential equation which deforms the initial level set, is given by

$$\frac{d}{dt}\phi = -\alpha \mathbf{A}(\mathbf{x}) \cdot \nabla\phi - \beta P(\mathbf{x})|\nabla\phi| + \gamma Z(\mathbf{x})\kappa|\nabla\phi| \tag{4}$$

where $\mathbf{A}$ is an advection term, P is a propagation term and Z is a spatial modifier term for the mean curvature κ [16]. The advection term $\mathbf{A}(\mathbf{x}) = -\nabla I_V(\mathbf{x})$ evolves the level set to the edges of the tumor. When the gradient of the speed function is negative, the level set expands. A positive gradient causes the level set to shrink. The propagation term $P(\mathbf{x}) = I_V(\mathbf{x})$ causes a speed dependent expansion of the level set and the curvature term $Z(\mathbf{x}) = I_V(\mathbf{x})$ reduces sharp edges in the level set.

2.4 Training

12 data sets of CT images of the abdomen from the university hospitals of Leuven are used for the training of the algorithm. For calculation of the minimal cost path, this training determines the relative weight of the external cost with respect to the internal cost. Besides that, parameter tuning of the weighting factors for the different terms for the level set equation (Eq. 4) is necessary to obtain the optimal results. Afterwards the tuned parameters are checked with the training data sets of "3D Segmentation in the Clinic: A Grand Challenge II" [10].

3 Results

Because the semi-automatic algorithm needs training, the results are discussed separately. The liver tumor data were acquired on one 64-slice and two 40-slice CT scanners using a standard four-phase contrast enhanced imaging protocol with slice thickness of 1 mm or 1.5 mm and an in-plane resolution of $0.6 - 0.9$ mm.

3.1 Validation

To evaluate the data, five measures are used: the overlap error (1 - volume overlap), the relative absolute volume difference between manual and semi-automatic segmentation, the average surface distance, the RMS surface distance and the maximum surface distance. Those measures are compared with an independent manual delineation by the organization of the challenge [10]. Based on this comparison a score is given to each evaluation measure and to each segmentation. A score of 90% means that the semi-automatic segmentation is as good as the manual delineation.

3.2 Training data

First, the parameters are tuned on 11 data sets of the university hospitals of Leuven containing 31 metastases. Afterwards, the first results of the semi-automatic liver tumor segmentation of the 10 clinical training data sets coming from 4 patients were assessed first visually and then quantitatively. Based on the visual inspection, the parameters of the level set method and the dynamic programming algorithm were further adjusted. To find the optimal parameters mainly the volume overlap was used.

The quantitative results for the training data are given in Table 2 and Table 3. The latter gives the surface distances in mm. There is made a distinction based on which surface is the reference surface. Calculating the total score using the same interobserver variability as the test data, gives a score of $79.1 \pm 9.2\%$. With a score of 92.3% for the average volume difference, this difference is smaller than the interobserver variability. This is not true for the scores of the other evaluation measures: 81.8% for the overlap error, 83.5% 70.6% and 67.1% for respectively the average, the RMS and the maximum surface distance.

3.3 Test data

The algorithm is tested by [10] on 10 tumors coming from 6 patients. The results of the test data are worse than the results of the training data, as can be seen in Table 1.

Table 1: Results (source: [10])

		Overlap Error		Volume Diff.		Ave. Surf. Dist.		RMS Surf. Dist.		Max. Surf. Dist.		
Patient	Tumor	(%)	Score	(%)	Score	(mm)	Score	(mm)	Score	(mm)	Score	Total Score
5	1	32,49	75	13.64	86	2.58	35	3.47	52	12.91	68	63
5	2	38.30	70	29.64	69	1.35	66	1.72	76	5.00	87	74
5	3	31.23	76	22.91	76	1.12	72	1.51	79	5.97	85	78
6	1	37.42	71	22.74	76	1.06	73	1.44	80	5.45	86	77
6	2	33.84	74	18.27	81	0.72	82	1.10	85	4.46	89	82
7	1	38.89	70	28.39	71	5.00	0	6.51	9	26.45	34	37
7	2	24.53	81	5.17	95	1.05	73	1.52	79	6.39	84	82
8	1	31.64	76	2.93	97	3.65	8	4.52	37	16.13	60	55
9	1	50.52	61	8.58	91	2.07	48	2.90	60	10.35	74	67
10	1	26.92	79	25.61	73	1.46	63	1.99	72	7.82	80	74
Average		34.58	73	17.79	82	2.01	52	2.67	63	10.09	75	69

The average total score $\pm$ standard deviation is $68.9 \pm 14.1\%$. The median is 74%. All average measures have a value below 90%,

4 Discussion

First, the effects of different aspects of the algorithm are discussed. The pixel classification algorithm actually searches the most probable tumor based on gray level intensities. Therefore, it can be seen as an optimization problem. To find the correct local optimum an accurate initialization is necessary. Deviations from

this most probable tumor are provided by the curvature term which forbids unnatural high curvatures in the segmentation. In [17] a 2D variant of the algorithm described here, is implemented and tested. The improvement of applying a level set method after the initial segmentation is an increase of the DSC of 1.5%.

By inverting the gradient when the tumor has higher intensity than the surrounding liver, the algorithm is able to segment dark and light tumor with respect to liver tissue. Another strength of the algorithm is the use of gray level intensities, gradients and local shape. Taking more tumor information into account, increases the reliability. Because the user has to define a maximum radius, the tumor won't grow out of the sphere with that radius.

On the other hand, the main shortcoming is the need that the tumor is surrounded by more or less homogeneous liver tissue. By adding a rest class, the pixel classification algorithm is capable to distinguish tissues with other gray levels from tumor tissue. Problems occur for tumor 2, patient 7. The tumor is adjacent to liver tissue and other structures in the abdomen. However, the worst results in Table 1 are mainly due to high surface distance errors. The cause is that those surface distances are not relative measures. In consequence big tumors have higher surface distance errors.

The discrepancy between the results of test and training data is remarkable. There are several possible explanations. Because we had no knowledge about the manual segmentation of the test data, user intelligence was reduced when placing the two seeds. In comparison to us, a physician does have that knowledge. In consequence he is capable to provide a qualitatively better segmentation. Another explanation could be that the tumors of the test data are inherently more difficult to segment.

An improvement could be obtained by implementing an efficient texture filter (see Fig. 1) which can increase the reliability of the pixel classification algorithm. Within the Haralick features [18], we suggest using correlation and variance, but also other features could be investigated. Another improvement of the pixel classification algorithm is adding outlier detection [19].

5 Conclusions

The semi-automatic algorithm described here is able to segment liver tumors by two user placed points. The tumor center and the maximum radius, both calculated from those two points, are used to provide a primary segmentation using the spiral-scanning technique. A level set method adjusts this first segmentation using a speed function obtained from a pixel classification algorithm. The accuracy is only sufficient in a small number of cases. The algorithm performs better for tumors that have an obvious edge, a high difference between the average gray level intensity of the tumor and the liver combined with a rather small standard deviation for both intensity distributions.

A Appendix: Details Results Training Data

Table 2: Results of training set

patient	tumor	DSC [%]	JSC [%]	Vol. Diff.[%]
1	1	62,42	45,37	3,15
	2	87,82	78,29	15,60
2	1	86,96	76,93	0,93
	2	87,83	78,30	9,17
	3	92,26	85,64	0,89
3	1	82,88	70,77	10,38
4	1	87,13	77,20	9,10
	2	89,96	81,75	14,20
	3	91,17	83,78	6,19
	4	92,62	86,26	4,13
av		86,11	76,43	7,37
std		8,82	11,87	5,19

Table 3: Results surface distances of training set

		manual			algorithm		
patient	tumor	SD_{mean}	SD_{max}	SD_{RMS}	SD_{mean}	SD_{max}	SD_{RMS}
1	1	-3,46	-13,29	5,23	-1,42	-16,59	6,46
	2	-1,57	-5,14	1,86	1,36	4,80	1,67
2	1	-1,31	-6,70	2,02	0,99	4,61	3,04
	2	-0,73	4,04	1,69	0,44	-6,76	1,82
	3	-1,08	-3,40	1,55	0,92	3,97	1,52
3	1	-1,88	-4,44	2,21	1,29	3,94	1,94
4	1	-0,88	-12,11	3,05	-0,02	8,29	2,98
	2	-0,72	-3,11	1,52	0,42	-3,53	1,59
	3	-1,70	-8,90	2,51	1,58	8,58	2,56
	4	-0,92	-4,64	1,71	0,82	5,32	1,73
av.		-1,42	6,57	2,33	0,64	6,64	2,40
std.		0,83	3,65	1,12	0,87	3,93	1,50

References

1. R. S. Tuma, "Sometimes size doesn't matter: Reevaluating RECIST and tumor response rate endpoints," *Journal of the National Cancer Institute*, vol. 98, pp. 1272–1274, September 2006.
2. S. Prasad, K. Jhaveri, *et al.*, "CT tumor measurement for therapeutic response assessment: comparison of unidimensional, bidimensional, and volumetric techniques initial observations," *Radiology*, vol. 225(2), pp. 416–9, November 2002.
3. L. N. Tran, M. S. Brown, J. G. Goldin, X. Yan, R. C. Pais, M. F. McNitt-Gray, D. Gjertson, S. R. Rogers, and D. R. Aberle, "Comparison of treatment response classifications between unidimensional, bidimensional, and volumetric measurements of metastatic lung lesions on chest computed tomography," *Academic Radiology*, vol. 11(12), pp. 1355–1360, Nov-Dec 2004.
4. E. Bellon, M. Feron, F. Maes, L. V. Hoe, D. Delaere, F. Haven, S. Sunaert, A. Baert, G. Marchal, and P. Suetens, "Evaluation of manual vs semi-automated delineation of liver lesions on CT images," *European Radiology*, vol. 7, p. 432438, 1997.
5. F. Maes, D. Vandermeulen, P. Suetens, and G. Marchal, "Computer-aided interactive object delineation using an intelligent paintbrush technique," in *Lecture Notes*

in Computer Science (N. Ayache, ed.), vol. 905, pp. 77–83, First Indernational Conference on Computer Vision, Virtual Reality and Robotics in Medicine, Springer, 1995.
6. F. Maes, D. Vandermeulen, P. Suetens, and G. Marchal, "Automatic image partitioning for generic object segmentation in medical images," in *Computational Imaging and Vision* (Y. Bizais, C. Barillot, and R. di Paola, eds.), vol. 3, pp. 215–226, XIVth International Conference on Information Processing in Medical Imaging, Kluwer Academic Publishers, 1995.
7. P. J. Yim and D. J. Foran, "Volumetry of hepatic metastases in computed tomography using the watershed and active contour algorithms," in *Proceedings of the 16th IEEE Symposium on Computer-Based Medical Systems*, IEEE Computer Society, 2003.
8. B. Zhao and D. Yankelevitz, "Two-dimensional multi-criterion segmentation of pulmonary nodules on helical CT images," *Medical Physics*, vol. 26(6), pp. 4678–4689, Juni 1999.
9. J. Wang, R. Engelmann, *et al.*, "Segmentation of pulmonary nodules in three-dimensional CT images by use of a spiral-scanning technique," *Medical Physics*, vol. 34(12), pp. 4678–4689, December 2007.
10. Medical Image Computing and Computer-Assisted Intervention, "3D segmentation in the clinic: A grand challenge II." http://grand-challenge2008.bigr.nl/, 2008.
11. V. Caselles, R. Kimmel, and G. Sapiro, "Geodesic active contours," *International Journal of Computer Vision*, no. 22 (1), p. 6179, 1997.
12. S. Osher and R. Fedkiw, *Level Set Methods and Dynamic Implicit Surfaces*. No. 153 in Applied Mathematical Sciences, Srpinger-Verlag New York, Inc., 2003.
13. P. Suetens, *Fundamentals of Medical Imaging*. New York: Cambridge University Press, 2002.
14. P. S. Kostka *et al.*, "Hybrid feature vector extraction in unsupervised learning neural classifier," *Engineering in Medicine and Biology*, vol. 1-4, pp. 5664–5667, September 2005.
15. S. Osher and N. Paragios, *Geometric Level Set Methods in Imaging,Vision,and Graphics*. Secaucus, NJ, USA: Springer-Verlag New York, Inc., 2003.
16. MeVis Research GmbH, "Me*VisLab*." http://www.mevislab.de.
17. D. Smeets and B. Stijnen, "The liver: 3D visualization and quantification of metastases," master thesis, Katholieke Universiteit Leuven: departement Elektrotechniek, biomedische technologie, June 2008.
18. R. M. Haralick, Dinstein, and K. Shanmugam, "Textural features for image classification," *IEEE Transactions on Systems, Man, and Cybernetics*, vol. SMC-3, pp. 610–621, November 1973.
19. K. Van Leemput, F. Maes, D. Vandermeulen, A. Colchester, and P. Suetens, "Automated segmentation of multiple sclerosis lesions by model outlier detection," Tech. Rep. 0004, KUL/ESAT/PSI, Heverlee, Belgium, Juni 2000.